Biology of Reproduction, 2024, **110(2)**, 391–407
https://doi.org/10.1093/biolre/ioad141
Advance access publication date 20 October 2023
Research Article

KDM6A/UTX promotes spermatogenic gene expression across generations and is not required for male fertility†

Benjamin W. Walters[1], Shannon R. Rainsford[1], Rachel A. Heuer[1], Nicolas Dias[1], Xiaofang Huang[2], Dirk de Rooij[3,4] and Bluma J. Lesch[1,5,6,*]

[1]Department of Genetics, Yale School of Medicine, New Haven, CT, USA
[2]Department of Cellular and Molecular Physiology, Yale School of Medicine, New Haven, CT, USA
[3]Reproductive Biology Group, Division of Developmental Biology, Department of Biology, Faculty of Science, Utrecht University, Utrecht, The Netherlands
[4]Center for Reproductive Medicine, Academic Medical Center, University of Amsterdam, Amsterdam, The Netherlands
[5]Department of Obstetrics, Gynecology and Reproductive Sciences, Yale School of Medicine, New Haven, CT, USA
[6]Yale Cancer Center, Yale School of Medicine, New Haven, CT, USA

*__Correspondence:__ 333 Cedar Street, New Haven, CT 06510 USA. E-mail: bluma.lesch@yale.edu

†__Grant Support:__ This work was supported by funding from the National Institutes of Health/National Institute of Child Health and Human Development (R01HD098128), by a Career Enhancement Program Grant from the Yale SPORE in Lung Cancer (P50CA196530), by a Pew Biomedical Scholar Award from the Pew Charitable Trusts to BJL (GR-000010759). BWW is a Hope Funds for Cancer Research Fellow supported by the Hope Funds for Cancer Research (HFCR 22-03-04).

Abstract

Paternal chromatin undergoes extensive structural and epigenetic changes during mammalian spermatogenesis, producing sperm with an epigenome optimized for the transition to embryogenesis. Lysine demethylase 6a (KDM6A, also called UTX) promotes gene activation in part via demethylation of H3K27me3, a developmentally important repressive modification abundant throughout the epigenome of spermatogenic cells and sperm. We previously demonstrated increased cancer risk in genetically wild-type mice derived from a paternal germ line lacking *Kdm6a* (*Kdm6a* cKO), indicating a role for KDM6A in regulating heritable epigenetic states. However, the regulatory function of KDM6A during spermatogenesis is not known. Here, we show that *Kdm6a* is transiently expressed in spermatogenesis, with RNA and protein expression largely limited to late spermatogonia and early meiotic prophase. *Kdm6a* cKO males do not have defects in fertility or the overall progression of spermatogenesis. However, hundreds of genes are deregulated upon loss of *Kdm6a* in spermatogenic cells, with a strong bias toward downregulation coinciding with the time when *Kdm6a* is expressed. Misregulated genes encode factors involved in chromatin organization and regulation of repetitive elements, and a subset of these genes was persistently deregulated in the male germ line across two generations of offspring of *Kdm6a* cKO males. Genome-wide epigenetic profiling revealed broadening of H3K27me3 peaks in differentiating spermatogonia of *Kdm6a* cKO mice, suggesting that KDM6A demarcates H3K27me3 domains in the male germ line. Our findings highlight KDM6A as a transcriptional activator in the mammalian male germ line that is dispensable for spermatogenesis but important for safeguarding gene regulatory state intergenerationally.

Summary Sentence

The histone demethylase KDM6A (also called UTX) is expressed transiently just before and during meiotic entry in spermatogenesis and is important for maintaining epigenetic state transgenerationally in the male germ line.

Received: July 10, 2023. **Revised:** September 26, 2023. **Accepted:** October 19, 2023

Graphical Abstract

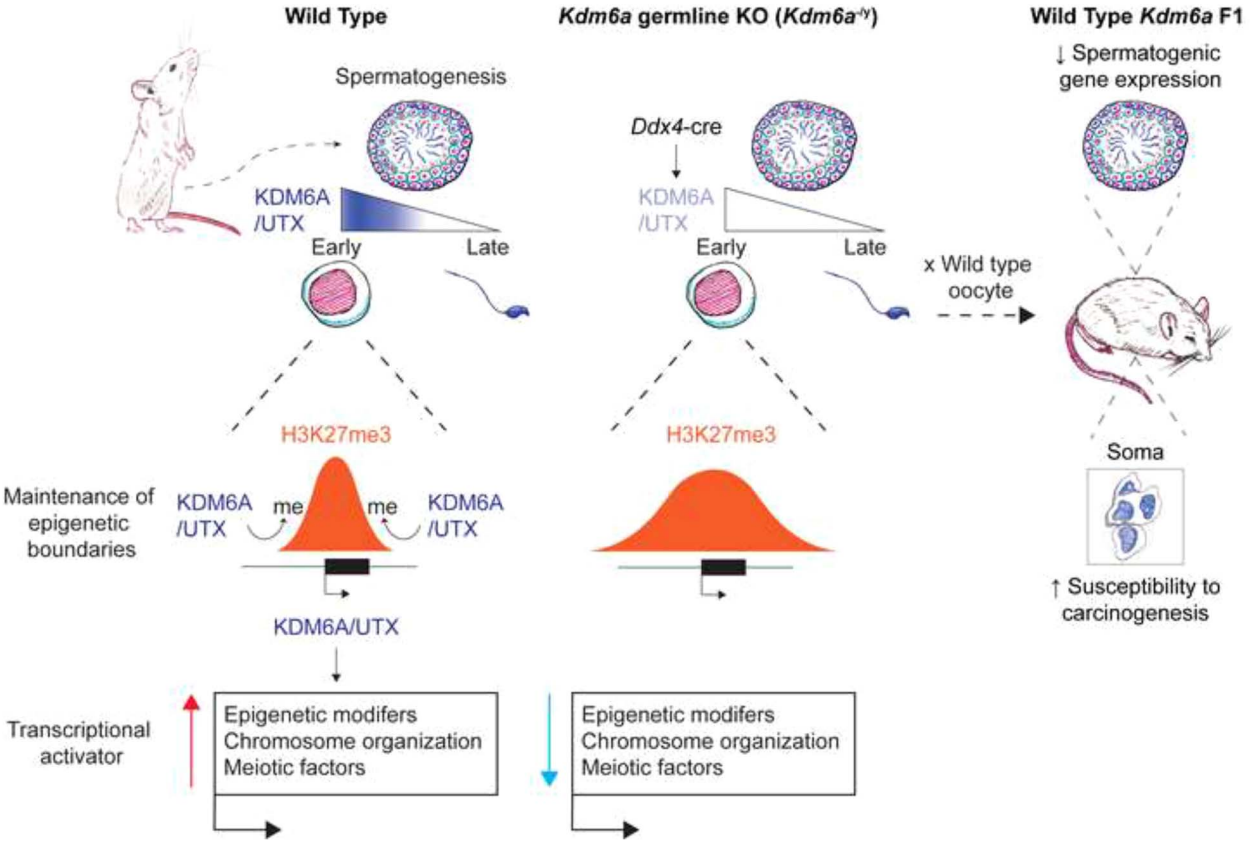

Key words: spermatogenesis, epigenetics, chromatin, transgenerational, KDM6A, UTX

Introduction

Chromatin state is a major determinant of gene expression. Posttranslational histone modifications play a central role in defining and regulating chromatin state, and histone modifying enzymes are critical factors in guiding gene expression programs. The importance of histone modification dynamics is particularly evident in spermatogenesis, during which chromatin is dramatically remodeled and modified to facilitate precise temporal gene expression programs and to generate a viable epigenome for the next generation. One of the best characterized histone modifications in the male germ line is trimethylation of histone H3 at lysine 27 (H3K27me3), which is catalyzed by Polycomb repressive complex 2 (PRC2) [1, 2]. Extensive studies in multiple cell types point to a role for PRC2 and H3K27me3 in limiting promiscuous gene expression. For example, H3K27me3 is enriched at a large set of genes encoding developmental regulators in mouse embryonic stem cells, where its presence supports ground-state pluripotency [3, 4]. In male germ cells, loss of PRC2 leads to derepression of somatic and stage-specific meiosis genes and ultimately causes sterility [5]. H3K27me3 is also one of the two modifications that define bivalency, a unique chromatin state defined by co-occupancy with the activation mark H3K4me3 and thought to poise repressed germline genes for later activation in the developing embryo [6–11]. Several studies have linked paternally derived H3K27me3 epimutations with detrimental developmental consequences in offspring [12–15]. Therefore, modulation of the levels and distribution of H3K27me3 is critical for male germ line function and for ensuring appropriate offspring development.

The X-linked gene Lysine Demethylase 6a (*Kdm6a*, also known as *Utx*) counterbalances PRC2 activity by demethylating H3K27me2/3 to derepress genes and promote transcription [16–18]. KDM6A was initially described as a critical developmental factor in *Caenorhabditis elegans* and zebrafish through its regulation of *HOX* gene activation [17, 18]. KDM6A has since been shown to play important roles in diverse cellular processes, including embryonic stem cell differentiation, aging, cellular reprogramming, development, and cancer [19–30]. In addition to the catalytic activity of KDM6A toward H3K27me3 at promoters, KDM6A also plays a non-catalytic role in regulating enhancer activation as part of the MLL3/4 complex [31, 32]. KDM6A thus has multiple roles as a transcriptional regulator in establishment of gene expression programs.

Missense and truncating mutations in *KDM6A* have been identified across a broad range of human cancers, suggestive of a function for KDM6A as a tumor suppressor [33]. Loss of *Kdm6a* in the mouse paternal germ line potentiates cancer risk in genetically wild-type offspring, implying that some of the tumor suppressive effects of KDM6A are heritable [14]. This phenotype suggests a model in which KDM6A either primes the sperm epigenome with gene regulatory information that can be passed to somatic tissues of offspring to limit

malignant transformation or removes regulatory information whose aberrant transmission to offspring promotes tumorigenesis. How KDM6A functions during spermatogenesis in the father to confer these effects in the next generation is not fully understood.

In this study, we aimed to define the cellular and molecular changes that occur upon deletion of *Kdm6a* in the male germ line and identify candidate pathways that could participate in the cancer risk observed in offspring. We show that *Kdm6a* expression is largely limited to differentiating spermatogonia and the early stages of meiotic prophase, in contrast to the broad expression of most histone demethylase genes during spermatogenesis. KDM6A acts as a transcriptional activator predominantly during this important transition period in spermatogenesis, affecting a large set of genes including many encoding chromatin remodelers and regulators of chromosome organization. Loss of KDM6A does not substantially change which loci are marked by H3K27me3, but rather enforces the boundaries of H3K27me3 domains. Loss of *Kdm6a* does not overtly impact the progression of spermatogenesis, although we observed a mild increase in sperm head defects. Intriguingly, we identified a subset of genes positively regulated by KDM6A that were persistently downregulated in the testes of wild-type offspring of *Kdm6a* cKO males. Overall, our data support a model in which KDM6A restricts accumulation of epigenetic information in the male germ line and where failure to restrict this information is compatible with fertility but can alter gene expression across generations.

Materials and methods

Mouse breeding and animal care

All mice were maintained on a C57BL/6J genetic background. To obtain *Kdm6a* cKO males, *Kdm6a*$^{flox/flox}$ (*Kdm6a*$^{tmc1(EUCOMM)Jae}$) females were mated with mice carrying one copy of the *Ddx4*-Cre transgene (B6-*Ddx4*$^{tm1.1(cre/mOrange)Dcp}$) [34, 35] in which Cre is expressed specifically in germ cells beginning at embryonic day 15.5. *Kdm6a* F1 males were generated by crossing male *Kdm6a* cKO mice with wild-type females. *Kdm6a* F1 cKO males were generated by breeding male *Kdm6a* cKO mice with female *Kdm6a*$^{flox/+}$ mice, and these were then crossed with wild-type females to generate wild-type *Kdm6a* F2 males. Primers used for genotyping are listed in Table S1. These studies were approved by the Yale University Institutional Animal Care and Use Committee under protocol 2020-20169. All mice used in these studies were maintained and euthanized according to the principles and procedures described in the National Institutes of Health guide for the care and use of laboratory animals.

GC-1spg culture and transduction

GC-1spg cells (ATCC, CRL-2053) were cultured in DMEM (Gibco, 11965092) supplemented with 10% fetal bovine serum (Corning, 35-011-CV), 1 mM sodium pyruvate (Gibco, 11360-070), and pen-strep (Gibco, 15140-122). At 90% confluency, cells were passaged 1:15 every 3 days using trypsin (Gibco, 25300054) and centrifugation at 200 × *g*. *Kdm6a* knockdown cell lines were generated by lentiviral transduction of shRNAs expressed from a pZIP-mEF1α-ZsGreen-Puro lentiviral vector (TransOMIC Technologies) in the presence of 8 μg/ml polybrene. Three days after transduction, the cells were treated with 2 μg/ml puromycin for a week to select for stable transductants. Sequences for shRNA constructs can be found in Supplementary Table S1. MycoStrip (InvivoGen, rep-mys-10) did not detect mycoplasma contamination in any of the cell cultures used in this study.

Immunoblotting

Whole cell lysates were prepared using RIPA buffer supplemented with 0.9% SDS. Subcellular fractions were prepared according to Gagnon et al. [36]. Up to 40 μg of total protein was loaded onto a Mini-PROTEAN TGX gel (Bio-Rad, 456-8093) and separated by SDS-PAGE for 1 h at 200 V. Separated proteins were then wet transferred to a 0.45-μm nitrocellulose membrane (GE Healthcare Life Science, 10600003) in Towbin buffer (25 mM Trizma base, 192 mM glycine, 20% (v/v) methanol) at a constant current of 250 mA for 1 h. The membrane was then briefly incubated in Ponceau S (Sigma Aldrich, P7170), washed in TBST, then blocked in 5% w/v non-fat dry milk (American Bio, ab10109-01000) in TBST for 30 min with gentle agitation at room temperature. Primary antibodies were diluted in blocking buffer and incubated with the membrane overnight at 4°C with gentle rocking. After washing in TBST, the membranes were incubated with peroxidase-conjugated secondary antibodies diluted 1:10 000 in blocking buffer. Following washing, the membrane was incubated for 5 min in SuperSignal West Pico Plus (Thermo, 34580) or the Femto variant (Thermo, 34096), and the signal was captured with X-ray film (Thermo, 34090). Antibodies used for immunoblotting are listed in Table S2.

Tissue staining

Mouse testes were dissected and immersed in Hartman's fixative for 30 min at room temperature before bisecting for further fixation overnight at 4°C on an end-to-end rotator. Fixed testes were subjected to standard dehydration and clearing processing for paraffin embedding. Wax sections were stained with hematoxylin and eosin for histological analysis and indirect immunofluorescence was performed after 20 min of heat-induced epitope retrieval with citrate buffer (Vector Laboratories, H-3300). Confocal images were taken using a Zeiss LSM 880 microscope. Antibodies used for immunostaining are listed in Table S2. In situ hybridization was performed using RNAscope 2.5 HD assay—RED (ACDBio, 322360) according to the manufacturer's instructions. The assay was optimized by performing heat-induced antigen retrieval for 15 min and protease III digestion for 30 min at room temperature.

Testis cell dissociation

Decapsulated testes were incubated in DMEM containing 0.75 mg/ml collagenase type IV (Gibco, 17104-019) for 10 min at 37°C with occasional inversion. Equal volume of DMEM was added to the suspension of dissociated tubules before centrifuging at 400 × *g* for 5 min at 4°C. After removing the supernatant, the cell pellet was washed in DMEM and resuspended in accutase (Gibco, A1110501) for subsequent CUT&Tag analysis or 0.05% trypsin–EDTA (Gibco, 25200-056) for other analyses for 10-min incubation at room temperature. An equal volume of ice-cold DMEM + 10% FBS was then added to the cell suspension before washing the pellet twice with media. The cell pellet was resuspended in DPBS (Sigma, D8537) containing 0.04% bovine serum albumin (Sigma, A9647) and filtered through a

100-μm filter (Falcon, 22363549) then a 40-μm filter (Falcon, 352340) to generate a single-cell suspension.

Spermatogonia enrichment by flow cytometry

Dissociated germ cells were incubated in the dark for 20 min with PE conjugated anti-cKIT at 1:500 (Thermo, 12-1171-82) on ice. Stained cells were then washed twice, resuspended in complete media and sorted on a two-laser (466 and 561 nm) cell sorter (Bio-Rad S3e) as previously described [37]. Briefly, debris was removed from the plot based on FSC-A/SSC-A and singlets were selected based on FSC-H/FSC-A. A histogram of FL2-A was used to identify positively stained cells compared to an unstained aliquot.

Pachytene spermatocyte and round spermatid enrichment by STA-PUT

STA-PUT was performed as described in Bellvé [38]. For each isolation, six to eight testes from adult wild-type mice were pooled and washed twice in Dulbecco modified Eagle medium (DMEM). A linear gradient was generated using 350 ml of 2% BSA and 350 ml of 4% BSA solutions in the corresponding chambers. Approximately 1×10^8 dissociated male germ cells were resuspended in 20 ml of 0.5% BSA solution and loaded to the sedimentation chamber. After 3 h of sedimentation, 60 fractions were collected in 15-ml centrifuge tubes and numbered sequentially 1–60. Cells from each fraction were collected by centrifugation at $500 \times g$ for 5 min and resuspended in 0.2 ml total volume. An aliquot of each fraction was stained with Hoechst dye (Invitrogen, H3570) and examined thoroughly by eye under phase-contrast and fluorescence microscopes to assess cellular integrity and identify cell types. Fractions containing >80% cells of appropriate size and morphology were pooled as pachytene spermatocytes and round spermatids. Final purity was estimated at 85% for meiotic and 90% for postmeiotic populations based on visual examination of bright-field and Hoechst-stained cells.

Morphological assessment of spermatozoa

Cauda epididymides were dissected from adult male mice and cut into 1 ml of warm M2 medium (Sigma, M7167) to allow sperm to swim out. After 15 min, the cell suspension was centrifuged for 2 min at $2000 \times g$ at 4°C and the resulting pellet was resuspended in 4% paraformaldehyde for 20 min at room temperature. Fixed spermatozoa were pelleted and washed twice in 100 mM ammonium acetate before resuspending in 150 μl wash buffer. Five microliters of this cell suspension was spread across a glass slide and air dried followed by Coomassie staining for 10 min. After rinsing in tap water, the slides were air dried then coverslipped with DPX (Sigma, 06522). The percentage of sperm with abnormal heads was visually assessed from >400 sperm for each biological replicate using bright-field microscopy under blinded conditions.

Motility assessment of spermatozoa

Cauda epididymal sperm were collected by swim-out (described above) and aliquots were placed in a slide chamber (Cell Vision, 20 mm depth). Motility was examined on a 37°C stage of a Nikon E200 microscope under a 10× phase-contrast objective (CFI Plan Achro 10×/0.25 Ph1 BM; Nikon). Images were recorded (40 frames at 50 fps) using a CMOS video camera (Basler acA1300-200 μm; Basler AG, Ahrensburg, Germany) and analyzed by computer-assisted sperm analysis (CASA, Sperm Class Analyzer version 6.3; Microptic, Barcelona, Spain). Sperm total motility and hyperactivated motility were quantified simultaneously. Over 200 motile sperm were analyzed for each trial.

RNA isolation

For bulk RNA sequencing and RT-qPCR, total RNA was extracted from pelleted cells and dissected seminiferous tubules by homogenizing in 1 ml of TRIzol reagent (Invitrogen, 15596026). After 5 min of incubation, the lysate was mixed with 200 μl of chloroform and centrifuged at $12\,000 \times g$ for 15 min at 4°C. The aqueous phase was mixed with an equal volume of 100% ethanol and transferred to an RNeasy MinElute spin column (Qiagen, 74104) for purification according to the manufacturer's instructions. The quality of the eluted RNA was assessed by 28S/18S ribosomal ratios and RNA integrity number (RIN) using an Agilent Bioanalyzer.

Real-time quantitative PCR

Reverse transcription of 1 μg of total RNA was performed with oligo(dT) and SuperScript III reverse transcriptase (Thermo, 18080051) in a total volume of 20 μl according to the manufacturer's instructions. Reaction mixtures were incubated in a thermocycler at 65°C for 10 min then 50°C for 50 min before stopping the reaction at 85°C for 5 min. Real-time quantitative PCR (RT-qPCR) assays were performed in a total reaction volume of 20 μl consisting of 4 μl of cDNA diluted 1:5, 0.4 μl of 10 μM forward/reverse primer mix, 10 μl of Power SYBR Green PCR Master Mix (Applied Biosystems, 4367659), and 5.6 μl nuclease-free water. Reactions for each target gene were performed in duplicate in a 96-well plate loaded into an Applied Biosystems QuantStudio 3 Real-Time PCR system. Standard cycling conditions were used: hold stage (×1): 50°C for 2 min, 95°C for 10 min; PCR stage (×40): 95°C for 15 s, 60°C for 1 min. Melt curve stage conditions were 95°C for 15 s, 60°C for 1 min, and 95°C for 15 s. Relative fold change in transcript abundance was calculated using the delta–delta Ct method by normalizing target gene expression levels to *Actb*. Primer sequences used for RT-qPCR are listed in Table S1.

Bulk RNA sequencing and analysis

Poly(A)-selected RNA-seq libraries were sequenced to a depth of ~25 million read pairs per sample. Raw sequence files were filtered and their quality was assessed using FASTX-toolkit and FastQC. Filtered paired-end reads were matched to yield a file of common reads which were then pseudoaligned to the mouse (mm10) transcriptome [39] and quantified using Kallisto v0.45.0 [40]. Resulting transcript counts were summed to gene level and differentially expressed genes were called using DESeq2 [41]. Genes with <10 TPM were filtered from the analysis. Genes with P values ≤ 0.05 were considered differentially expressed. A fold change cut-off of ≥ 1.5 was used to define strongly differentially expressed genes.

Single-cell RNA sequencing and analysis

Raw count matrices from mm10 were generated by CellRanger (10X Genomics) for the control ("WT") and conditional *Kdm6a* knockout ("cKO") mouse samples and imported to Seurat 4.1.0 [42] and combined into one

Seurat object. There were 19,378 cells detected in the "WT" sample and 16,740 cells in the "cKO." No explicit integration step was performed because principal component analysis (PCA) indicated high initial similarity between samples. Reads were filtered to exclude cells likely to be doublets (nCount_RNA < mean + 1 SD), dead or dying cells (nFeature_RNA > mean − 1 SD), or high mitochondrial content (percent.mt < mean + standard deviation). This resulted in a total of 15,325 cells for "WT" and 11,587 cells for "cKO." This filtered subset was log normalized and scaled. A linear dimensional reduction was performed using PCA, and 20 dimensions was chosen as optimum based on inspection of the "ElbowPlot()" function. Clusters were identified at a resolution of 0.5, and the "RunUMAP()" function was used to create Uniform Manifold Approximation and Projection (UMAP) objects. Clusters were characterized by key spermatogenic genes to identify cell type. Three of the initial clusters had a low number of detected molecules per cell, indicating dead or dying cells, and did not have any top genes associated with the transition from spermatogonia to elongating spermatid. Therefore, these three clusters were removed, resulting in 8619 cells for the "WT" sample and 7790 cells for the "KO" sample. The data were normalized, scaled, and dimensionally reduced again using the same parameters described above. Cluster identities were again assigned using key spermatogenic genes. Differentially expressed genes for each cluster were determined using the "FindMarkers()" function. All graphs were produced in R using the ggplot2 package.

CUT&Tag library preparation

CUT&Tag libraries were prepared using the Active Motif anti-Rabbit assay kit (Active Motif, 53160) with minor amendments to the manufacturer's protocol. Briefly, cKIT+ cells were sorted from dissociated testis and centrifuged at 1000 × *g* for 3 min at room temperature before washing the cell pellet in the buffer provided. For each reaction, 50 μl of cell suspension (50 000 cKIT+ cells) was incubated with 6 μl of concanavalin A beads in a 0.5-ml tube. After 10 min, the beads were captured using a magnetic stand and resuspended in 50 μl of antibody buffer containing PIC, digitonin, and 1 μg of primary antibody (see Table S2). After overnight incubation at 4°C, the liquid was removed, and the beads were incubated at room temperature for 60 min with 50 μl of secondary antibody diluted in Dig-wash buffer. The beads were then washed once with 500 μl Dig-wash buffer before incubating with 50 μl of diluted transposomes for 60 min. After a single wash with 500 μl of Dig-300 buffer the beads were incubated with 125 μl of Tagmentation buffer for 60 min in a thermomixer set at 400 rpm 37°C. The DNA was then extracted and PCR amplified according to the manufacturer's instructions. Finally, SPRI bead clean-up was performed before eluting purified DNA into 16 μl elution buffer.

CUT&Tag sequencing and analysis

An Agilent 2100 Bioanalyzer using a high sensitivity DNA assay kit was used to assess the quality of prepared libraries, which were then paired-end sequenced to achieve ∼30 million reads. For computational analysis, we performed quality filtering of fastq files using FASTX-Toolkit [43]. The adapter sequences (CTGTCTCTTATACACATCT) were trimmed for each filtered file using cutadapt [44] and Seqkit was then used to match paired reads [45]. Reads were then aligned to the mm10 mouse genome assembly using Bowtie2 with –end-to-end –very-sensitive settings enabled [46]. The sequencing depth was equalized across all samples and the resultant .sam file was converted to bam files. After sorting and indexing using SAMtools [47] the bam files were converted to bigwig format using bamCoverage [48]. We generated metagene plots from the bigwig files using deepTools [48]. Peak calling was performed using SEACR [49].

Chromatin accessibility analysis

Chromatin accessibility was assayed with 100 000 cells per sample. Libraries were prepared using the Active Motif ATAC-Seq kit (53150) according to the manufacturer's instructions except 11 PCR cycles were used instead of the recommended 10 cycles. Libraries were sequenced to a depth of ∼50 million paired-end 100 bp reads per sample. Adapter trimming was performed using Cutadapt [44]. Trimmed reads were aligned to the mouse genome (mm10) using Bowtie2 in very sensitive mode [46]. Subsequent processing was performed according to the *csaw* workflow previously described in [50]. Regions of differential chromatin accessibility were called using *csaw* workflow "method IV." Briefly, reads were counted at regions corresponding to the union of peaks identified by default parameters in MACS2 for control and knockdown/knockout samples. Then, low abundance windows were filtered and a nonlinear loess-based normalization method was implemented. Resulting count matrices were then subjected to *edgeR* [51] for differential accessibility quantification.

Functional enrichment analysis

Gene Ontology enrichment analysis was performed using PANTHER GO annotations (https://doi.org/10.5281/zenodo.4495804 released: 1 February 2021) at the GO Consortium website [52] (http://www.geneontology.org). Genes considered to be expressed (i.e., >1 TPM) in the relevant sample type were used as the reference list. Gene Set Enrichment Analysis (GSEA) was conducted as previously described using version 4.2.3 with default parameters [53, 54].

Repetitive element expression analysis

Repeat element expression was analyzed using RepEnrich2 [55]. Briefly, we built repeat element annotation files including all repeat elements except simple and low-complexity repeats. Read files were aligned to mm10, and RepEnrich2 was used to output estimated repeat element read counts. Output files were processed and input to DESeq2 for differential expression analysis. We called differentially expressed repeat elements between control and *Kdm6a* cKO mice, as well as between the control F1 and the wild-type F1 and F2 offspring of *Kdm6a* cKO mice ($P \leq 0.05$).

Statistical analysis

Statistical significance was determined at a threshold of $P < 0.05$ using an unpaired *t*-test for parametric and Wilcoxon rank-sum test for nonparametric data, or as specified in the appropriate figure legend. For comparison of CUT&Tag read counts in Figure 4I and J, data were modeled with a quasi-Poisson regression using the formula: glm(reads ∼ condition + locus, data, family = quasipoisson, link = "log"). Quasi-Poisson regression was used to account for overdispersion while modeling counts data with a Poisson model [56]. Differences were considered statistically

significant for the "condition" (control vs. cKO) term at $P < 0.05$.

Results

KDM6A is transiently enriched in spermatogenic cells immediately before and during meiotic entry

Although *Kdm6a* was reported to be ubiquitously expressed in mice, including in reproductive organs [57], its expression pattern across adult spermatogenesis has not been carefully defined. To address this question, we first assessed levels of KDM6A protein in whole testis and in populations of meiotic (pachytene spermatocyte) and postmeiotic (round spermatid) cells enriched by STA-PUT [38] after validating antibody specificity in vitro using KDM6A-depleted spermatogonia-derived cells (GC1) [58] (Figure S1A). KDM6A protein was readily detectable in whole testis lysates but only weakly present in meiotic and postmeiotic cell lysates (Figure 1A), suggesting that a different population of somatic or germ cells expresses KDM6A at a level higher than either pachytene spermatocytes or round spermatids. To more precisely identify the cell type that normally expresses *Kdm6a* most strongly in wild-type adult testes, we generated a single-cell RNA-seq (scRNA-seq) data set from wild-type and *Kdm6a* cKO adult testes and examined the dynamics of *Kdm6a* gene expression across spermatogenic development in wild-type animals. After quality filtering the data set (see Materials and Methods, Figure S1B–G), we applied graph-based clustering with Seurat [42] to define 17 distinct clusters comprising 8619 wild-type and 7790 *Kdm6a* cKO cells representing the known trajectory of spermatogenic maturation along with most testicular somatic cell types, with the exception of Sertoli cells (Figures 1B and S2A; see below for *Kdm6a* cKO data). Consistent with our protein analysis, our wild-type scRNA-seq data revealed that *Kdm6a* expression is not uniform across testicular cell types. *Kdm6a* was lowly expressed in somatic cell populations, including macrophages, Leydig cells, and telocytes. Among germ cells, *Kdm6a* mRNA expression was almost exclusive to a defined developmental interval encompassing late spermatogonia and the early stages of meiotic prophase (Figure 1B). Publicly available scRNA-seq data sets from mouse [59] and human [60] confirmed a similar expression profile (Figure S2B and C). To validate this expression pattern, we enriched for late spermatogonia/early meiotic prophase germ cells from whole testes by flow cytometry for cells expressing the surface marker cKIT (cKIT+, Figure S2D) [61] and evaluated *Kdm6a* expression at the mRNA and protein levels by RT-qPCR and Western blotting. We confirmed a strong enrichment for *Kdm6a* mRNA relative to unsorted cells and relative to cKIT+ cells from a *Kdm6a* cKO animal (Figure 1C). At the protein level, we validated strong enrichment of KDM6A in the cKIT+ cell fraction relative to whole testis, pachytene spermatocytes, and round spermatids (Figures 1D and S2E) and relative to cKIT+ cells from a *Kdm6a* cKO animal (Figure S2F), after validating loss of KDM6A protein in *Kdm6a* cKO testes (Figure 1E). Further confirming this expression pattern, RNA in situ hybridization revealed an enrichment for *Kdm6a* transcript in the basal compartment of the seminiferous tubule where spermatogonia and early meiotic cell populations reside (Figures 1F and S2G), with enrichment particularly evident in stage IX–XII tubules containing spermatocytes in the early stages of meiotic prophase [62].

Kdm6a has two homologs in the mouse genome, *Uty* and *Kdm6b*. We queried our scRNA-seq data set to see if *Uty* and *Kdm6b* had similar gene expression patterns to *Kdm6a* and could be acting redundantly. *Uty* was weakly expressed in undifferentiated spermatogonia and early meiotic cells while *Kdm6b* expression was generally enriched in spermatogonia, indicating that both homologs are expressed in overlapping but not identical cell populations compared to *Kdm6a* in the adult mouse testis (Figure S3). To determine if the expression pattern of *Kdm6a* is unique, we also assessed the expression patterns of 17 other lysine demethylases using our scRNA-seq data. Seven lysine demethylases exhibited broad expression patterns across spermatogenesis, while 10 exhibited stage-specific expression profiles that did not fully overlap with *Kdm6a* (Figure S3). The expression pattern of *Kdm7b* was most similar to that of *Kdm6a* during early spermatogenesis but was also detectable in round spermatids. Interestingly, *Kdm7b* can demethylate mono- and di-methylated, but not tri-methylated H3K27 [63], implying that *Kdm6a* and *Kdm7b* may have complementary, non-redundant functions in regulating H3K27 methylation during spermatogenesis. We conclude that *Kdm6a* has a unique and transient expression pattern during spermatogenesis.

Overall, these data demonstrate that contrary to previous suggestions, *Kdm6a* expression is not ubiquitous in spermatogenesis. Instead, *Kdm6a* is temporally regulated during spermatogenesis and is most strongly expressed between the late stages of spermatogonial differentiation and the earliest stages of meiotic prophase, suggesting a potential function for KDM6A during meiotic entry.

Kdm6a is dispensable for spermatogenesis

To assess the role of KDM6A in spermatogenesis, we generated mice lacking *Kdm6a* specifically in germ cells (*Kdm6a* cKO). These mice carry a conditional allele of *Kdm6a* [28] along with the germ line-specific *Ddx4*-Cre [34, 35], resulting in deletion of the third *Kdm6a* exon and yielding a truncated non-functional protein specifically in the germ line [14]. In *Kdm6a* cKO males, *Kdm6a* mRNA and protein expression was undetectable in cKIT+ cells and whole testis lysates compared to control, confirming the efficacy of the knockout (Figures 1C and E and S2F). There was no change in the transcript levels of *Uty*, *Kdm6b*, or *Kdm7b* in *Kdm6a* cKO testes, indicating that KDM6A homologs are not compensating for *Kdm6a* loss at the transcript level (Figure S4A).

We next asked if *Kdm6a* loss in the male germ line caused any phenotypic abnormalities that might contribute indirectly to intergenerational differences in gene regulation. We previously showed that *Kdm6a* cKO males are normally fertile based on number of offspring [14]. We found that *Kdm6a* cKO testes were comparable in weight and size to control mice (Figures 2A and S4B), and there was no difference in number of cauda epididymal sperm (Figure 2B). Histologically, all major spermatogenic cell types were present and morphologically normal in *Kdm6a* cKO seminiferous tubules (Figure 2C). No significant difference in the number of preleptotene spermatocytes was detected by manual counting in testis sections stained with hematoxylin and eosin (Figure S4C). We detected a statistically significant but very modest increase in the numbers of type A spermatogonia in *Kdm6a* cKO testis sections relative to control (Figure S4D).

Overall protein levels and spatiotemporal expression of markers for spermatogonia (LIN28, SALL4, STRA8, and CHD4), spermatocytes (SYCP3), and general spermatogenic

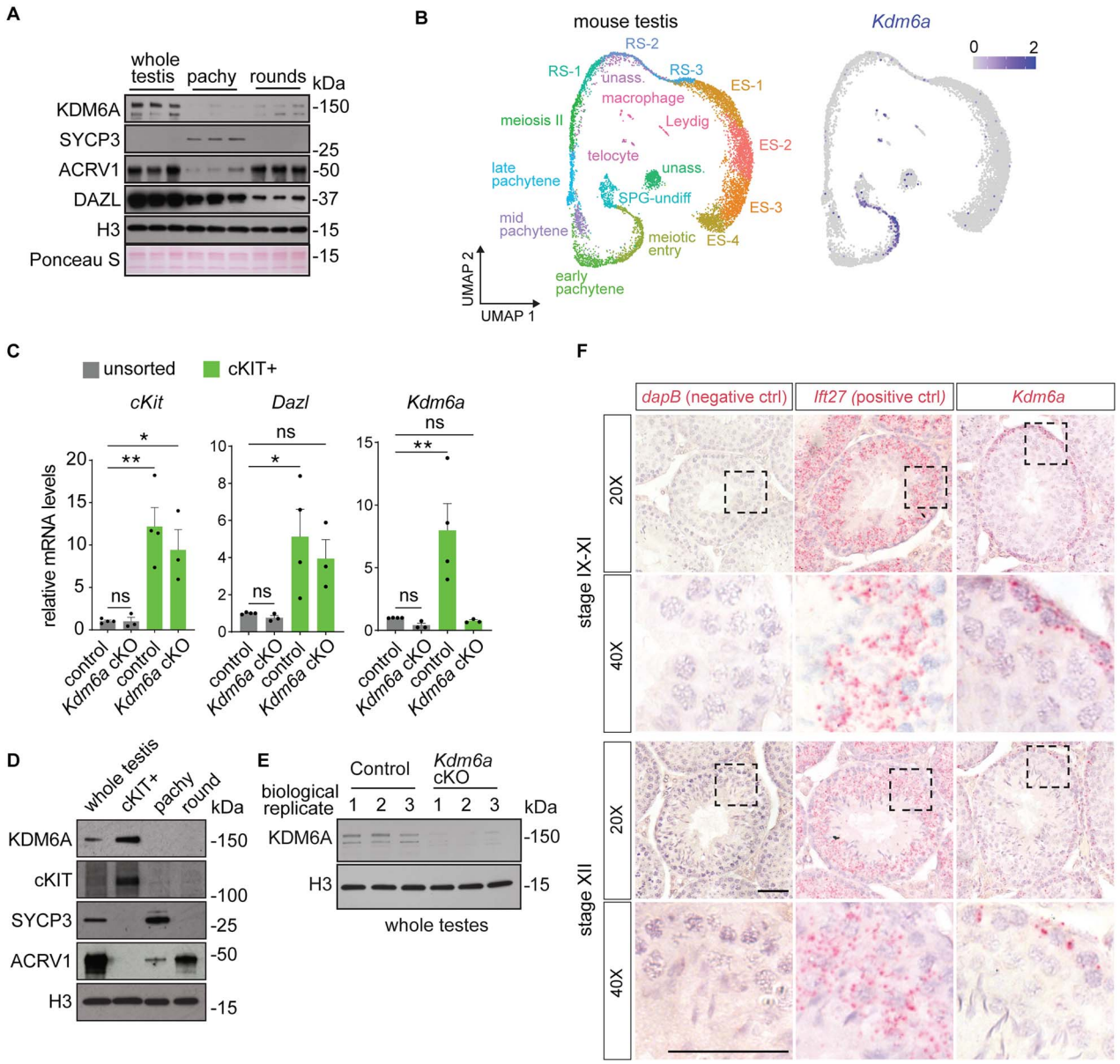

Figure 1. Expression analysis of KDM6A in the male germ line. (**A**) Western blotting in male germ cells for KDM6A and markers of meiotic (SYCP3) and postmeiotic (ACRV1) cells. DAZL is a general marker for germ cells and histone H3 is a loading control. (**B**) Left, UMAP of single-cell RNA-seq (scRNA-seq) data from whole mouse testis showing clustering and cluster identity assignments. Right, UMAP projection showing expression of *Kdm6a* across testis cell populations detected by scRNA-seq. (**C**) RT-qPCR in unsorted and cKIT-sorted cells derived from testes of control and *Kdm6a* cKO mice. ns = not significant, $^{*}P \leq 0.05$, $^{**}P \leq 0.01$ by one-way ANOVA with Dunnett post hoc test. (**D**) Western blotting for KDM6A in unsorted testis cells, cKIT+ cells, pachytene spermatocytes, and round spermatids. cKIT, SYCP3, and ACRV1 are markers for spermatogonia, spermatocytes, and round spermatids, respectively. H3 is a loading control. (**E**) Western blotting of whole testis lysates from control and *Kdm6a* cKO testes for KDM6A and histone H3 (loading control). (**F**) Bright-field micrographs showing in situ hybridization for the indicated transcript in tissue sections of seminiferous tubules co-stained with hematoxylin. Dashed boxes indicate the regions captured at high magnification below. Stage of the seminiferous epithelium is indicated. Scale bar = 50 μm.

cells (DAZL) were also comparable between control and *Kdm6a* cKO testes (Figures 2D and S4E). Gamma-H2AX (γH2A.X), a phosphorylated histone variant formed at sites of DNA damage and involved in meiotic recombination, meiotic sex chromosome inactivation, and meiotic silencing of unsynapsed chromatin, also exhibited similar cellular distribution patterns and global levels in *Kdm6a* cKO testes relative to control (Figures 2E and S4E), implying that these processes progress normally in the absence of KDM6A and that loss of KDM6A does not induce excess DNA damage in the male germ line.

Finally, we evaluated the form and function of mature spermatozoa. There was no motility defect in *Kdm6a* cKO sperm under capacitated and uncapacitated conditions as assessed by CASA [64] (Figure S4F). We detected a statistically significant but very modest increase in the fraction of *Kdm6a* cKO sperm with triangular shaped head defects (29%) relative to control (17%, Figure 2F) based on microscopic evaluation of Coomassie-stained sperm under blinded conditions. We conclude that KDM6A is dispensable for fertility and that there are no major spermatogenesis defects in *Kdm6a* cKO mice.

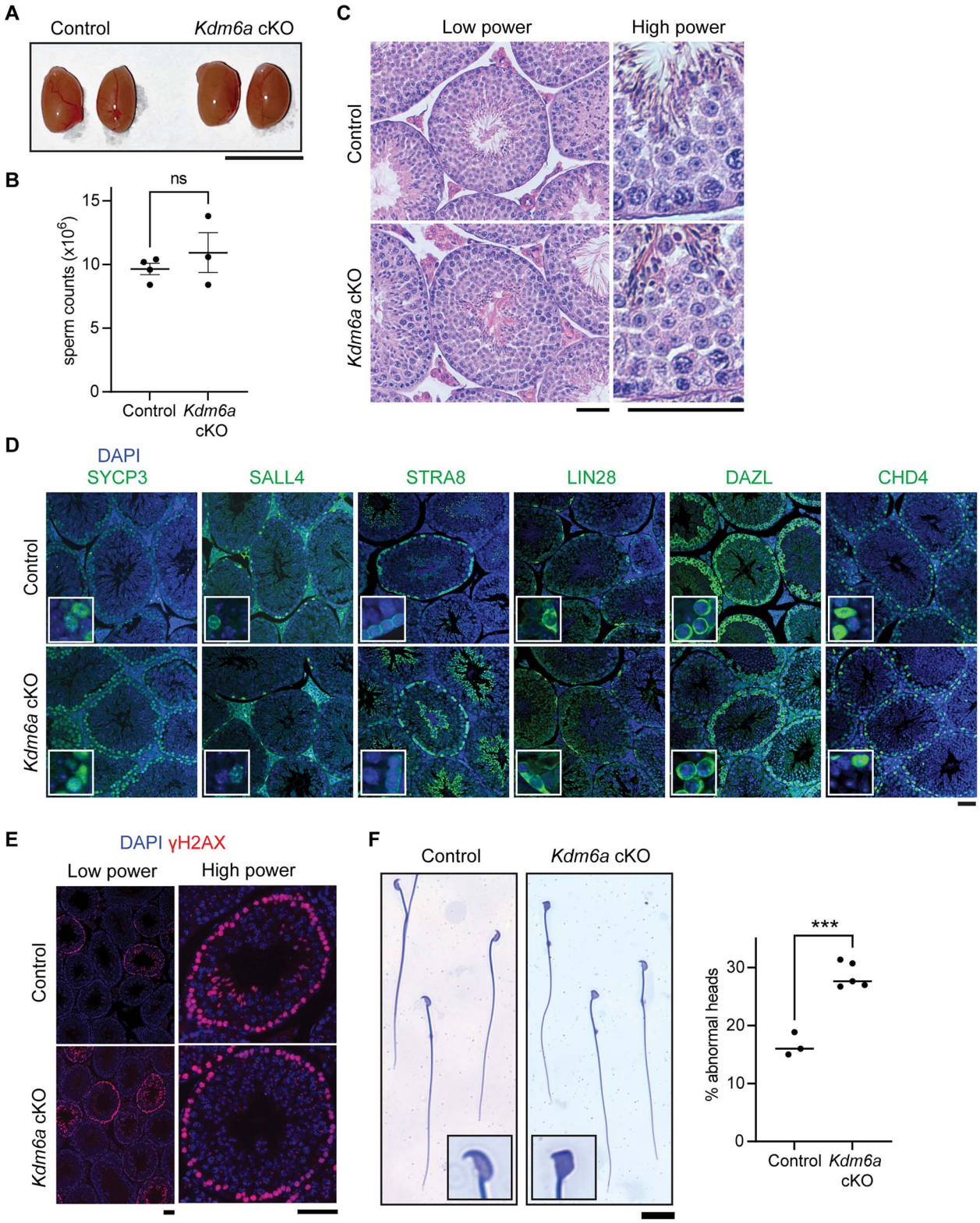

Figure 2. Minimal impact on spermatogenesis in *Kdm6a* cKO mice. (**A**) Gross morphology of testes from a control and a *Kdm6a* cKO mouse. Scale bar = 1 cm. (**B**) Epididymal sperm counts after swim-out in control ($n = 4$) and *Kdm6a* cKO ($n = 3$) mice. ns = not significant by unpaired *t*-test. (**C**) Cross-sections of control and *Kdm6a* cKO seminiferous tubules stained with hematoxylin and eosin. Scale bars = 50 μm. (**D**) Control and *Kdm6a* cKO testis sections immunostained for spermatogonia markers (LIN28A, STRA8, CHD4, and SALL4), a spermatocyte marker (SYCP3), and a general germ cell marker (DAZL) as well as DAPI to visualize DNA. Scale bar = 50 μm. (**E**) Immunofluorescence staining for γH2AX in sections from control and *Kdm6a* cKO testis. (**F**) Left, Coomassie-stained spermatozoa from control and *Kdm6a* cKO cauda epididymides; right, manual blinded quantification of abnormal heads. $^{***}P \leq 0.001$ by unpaired *t*-test. Scale bar = 20 μm.

KDM6A is a transcriptional activator in pre-meiotic male germ cells

Since KDM6A is not required for fertility, we next asked if KDM6A is important for regulation of gene expression during spermatogenesis that could have consequences for offspring phenotype. KDM6A is a positive regulator of transcription in mammalian cells through its H3K27 demethylase activity and its association with MLL3/4 complexes at promoters and enhancers [16–18, 31]. Therefore, we sought to define the genome-wide transcriptional effects of *Kdm6a* loss in the male germ line using our scRNA-seq data from *Kdm6a* cKO testis. There was no difference in overall spermatogenic developmental trajectory between control and *Kdm6a* cKO testes (Figures S1G and 3A), and the proportions of cells in each cluster were similar (Figure 3B), consistent with the absence of an infertility phenotype. Differential expression analysis across all clusters identified a total of 878 differentially expressed genes (scDEGs) in the *Kdm6a* cKO (Data set S1 and Figure 3C). The greatest number of scDEGs was found in cells where *Kdm6a* is most highly expressed ("meiotic entry" and "early pachytene" clusters) and detectable as a DEG ("meiotic entry" cluster), implying that these genes may be direct targets of KDM6A activity (Figures 3C and S5A). To support the scRNA-seq data, we also performed bulk RNA-seq in control and *Kdm6a* cKO whole testes ($n = 3$) and confirmed using GSEA [53, 54] that similar sets of genes exhibited altered expression in the whole-testis bulk data (Figure S5B). Deregulation of gene expression was strongly biased toward downregulation (76% of scDEGs, Figure 3D), consistent with the known function of *Kdm6a* in promoting expression of its targets. Upregulated scDEGs were enriched for Gene Ontology (GO) terms related to cytoplasmic translation, while downregulated scDEGs were more weakly enriched for several germ cell-related terms, the most significant being "spermatid development" (Figure 3E).

Based on the strong bias toward downregulation and known role of KDM6A as a positive regulator of gene expression, we focused our subsequent analysis on the downregulated scDEGs detected in *Kdm6a*-expressing cell populations ("meiotic entry" and "early pachytene" clusters) as they are the most likely candidates to be direct target genes of KDM6A. This subset of scDEGs was enriched for GO terms related to meiosis, sperm motility, histone modification, and chromosome organization (Figure 3F). Notably, while the expression of the homologs *Uty* and *Kdm6b* was unchanged, we found that 28 other chromatin modifiers were downregulated in *Kdm6a* cKO testis (Figure 3G) including other histone lysine demethylases (*Kdm1a*, *Kdm3a*, *Kdm5a*, *Kdm5b*, and *Kdm3c*) and ATP-dependent chromatin remodelers (*Smarcacc1*, *Smarca2*, and *Smarca5*). Eleven scDEGs have been implicated in the epigenetic regulation of repetitive elements, including several associated with the Human Silencing Hub (HUSH) complex [65, 66]. Interestingly, we found that 36% ($n = 65$) of downregulated scDEGs identified in the "ES-4" cluster ($n = 179$), representing the terminal stage of spermatogenesis (fully elongated and condensed sperm heads), were also called as scDEGs in the "meiotic entry" cluster (representing differentiated spermatogonia/early prophase, Figure S5C) and that these genes were significantly enriched for postmeiotic germ cell functions (Figure S5D). Thus, for some genes, KDM6A-mediated regulation may be the initial trigger for an expression state that is maintained by other factors throughout spermatogenesis, past the interval when KDM6A itself is expressed. We conclude that KDM6A promotes timely expression of genes related to chromatin organization during meiotic entry in the male germ line, and that loss of KDM6A leads to altered transcriptional states during meiotic entry as well as later in spermatogenesis.

KDM6A restricts H3K27me3 domain boundaries at meiotic entry

Based on the known role of KDM6A as a H3K27me2/3 demethylase [16–18, 67], we next evaluated the effects of loss of KDM6A on H3K27me3 distribution in differentiated spermatogonia and early spermatocytes. We confirmed that as expected, KDM6A protein was predominantly nuclear, indicating that the bulk of its activity is likely directed toward chromatin targets in the male germ line (Figure S6A). Global levels of H3K27me3 as assayed by Western blotting were unchanged in whole cell lysates of *Kdm6a* cKO cKIT+ cells compared to control (Figure 4A). Likewise, immunofluorescence in testis sections showed a similar distribution of H3K27me3 in the seminiferous tubules of *Kdm6a* cKO and control (Figure 4B).

The unchanged global levels of H3K27me3 suggested that loss of KDM6A might induce locus-specific changes in H3K27me3 in differentiating spermatogonia. We applied CUT&Tag [68] to evaluate H3K27me3 profiles across the genome in cKIT+ cells isolated by flow cytometry from control ($n = 2$) and *Kdm6a* cKO ($n = 3$) testes. Overall H3K27me3 CUT&Tag signal was highly reproducible between replicates, dissimilar to an IgG control sample from the same cell population, and comparable to ChIP-seq for H3K27me3 in cKIT+ cells (Figures 4C and S6B). H3K27me3 peaks called by SEACR [49] were similar in location, number, and length between control and *Kdm6a* cKO samples (Figures S6C and S6D). The majority of genes overlapping a H3K27me3 peak were similar, with 4393 overlapping targets (Figure 4D and Data set S2). H3K27me3 was lost ($n = 955$) or gained ($n = 781$) in *Kdm6a* cKO samples at a minority of genes (Figure 4D). Genes associated with both losses and gains were enriched for developmental functions when compared to the set of all genes, consistent with the known enrichment for H3K27me3 at developmental genes in pluripotent stem cells and germ cells (Figure 4E). However, only a small number of the genes that lost or gained H3K27me3 peaks were among the set of differentially expressed genes in *Kdm6a* cKO ($n = 44$, 5% of all scDEGs), and no functional enrichment was found when these genes were compared to a background of all H3K27me3-marked genes in cKIT+ cells, suggesting that changes in the location of H3K27me3 peaks are unlikely to account for the regulatory effects of KDM6A loss.

To assess more subtle differences in the level of H3K27me3 enrichment at specific loci, we then applied an established pipeline that accounts for the variability in signal background across replicates in genome-wide chromatin data [50]. This approach identified 710 loci with differential enrichment for H3K27me3, with a slight bias toward gain in signal in the *Kdm6a* cKO sample (Figure 4F). These differential peaks also marked genes associated with developmental functions (Figure 4G), but most of these genes were not differentially expressed in the *Kdm6a* cKO and no functional enrichment was found when compared against a background of all H3K27me3-marked genes in cKIT+ cells. These changes

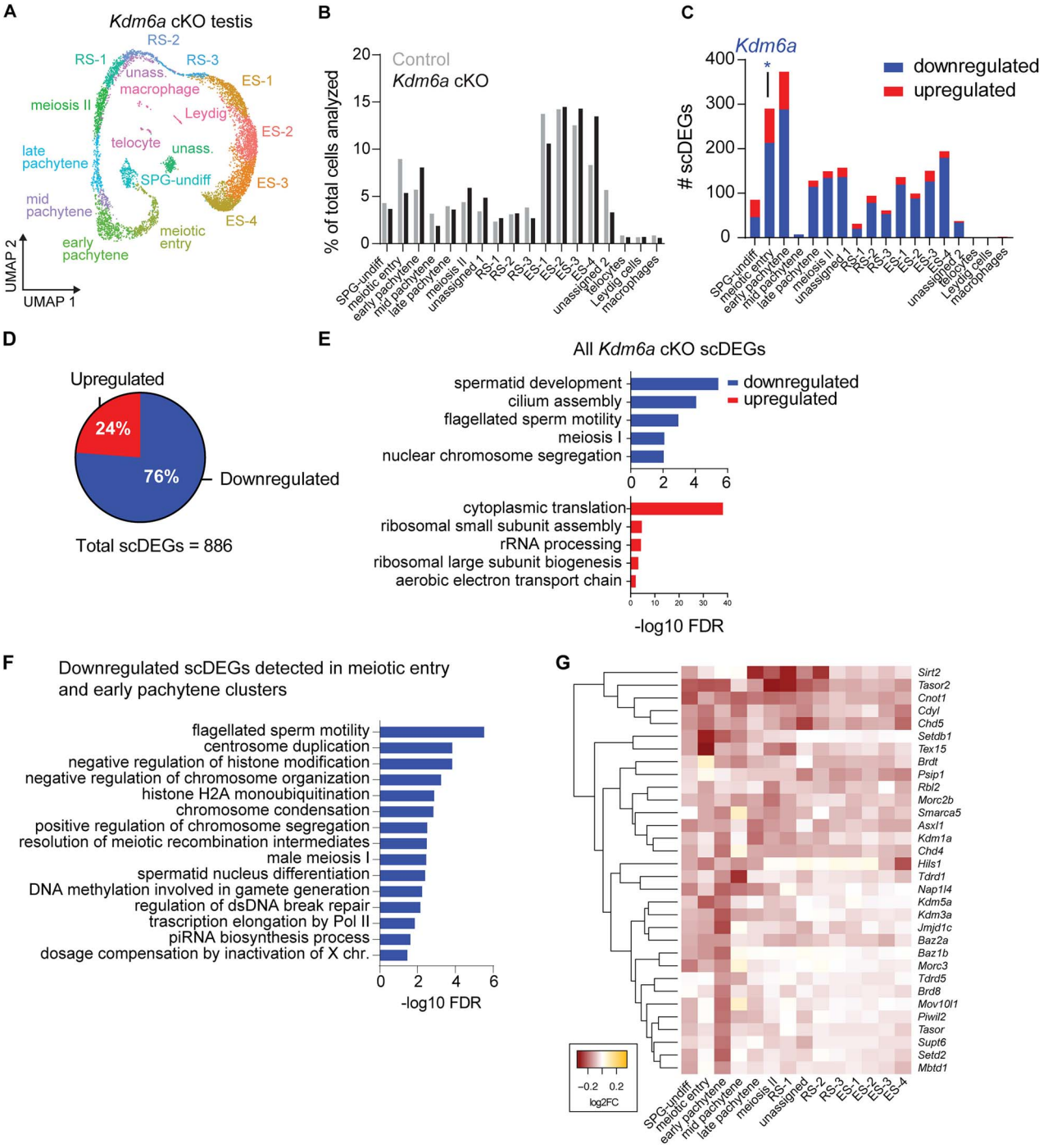

Figure 3. KDM6A promotes gene expression in spermatogenic cells. (**A**) UMAP and clustering for *Kdm6a* cKO scRNA-seq data set (see Figure 1B for equivalent control data). (**B**) Percentage of cells classified into each cluster out of total cells profiled in control and *Kdm6a* cKO scRNA-seq data sets. (**C**) Numbers of scDEGs identified per cluster. *Kdm6a* is identified as a scDEG in the "meiotic entry" cluster, which comprises differentiated spermatogonia and early stages of meiotic prophase. (**D**) Fraction of differentially expressed genes identified by scRNA-seq (scDEGs) that are downregulated and upregulated in *Kdm6a* cKO testis relative to control. (**E**) Gene Ontology analysis showing terms enriched in all downregulated and upregulated scDEGs identified in *Kdm6a* cKO testes. (**F**) Gene Ontology terms enriched in scDEGs identified for "meiotic entry" and "early pachytene" (cell populations spanning differentiated spermatogonia to early pachytene, corresponding to the timing of *Kdm6a* expression). (**G**) Heatmap displaying the gene expression changes (log2 fold change of *Kdm6a* cKO compared to control) for epigenetic modifiers and regulators of repetitive elements across clusters. Key is located at bottom left.

were also small in magnitude and thus unlikely to account for *Kdm6a*-dependent changes in gene regulation during spermatogenesis.

Finally, we assessed changes in the distribution of H3K27me3 signal, focusing on H3K27me3 peaks identified in wild-type cKIT+ cells. We observed a modest but consistent expansion of H3K27me3 in *Kdm6a* cKO samples, along with a slight decrease in signal at the peak summit (Figure 4H). This apparent broadening and flattening of H3K27me3 signal is consistent with a noisier distribution of this histone

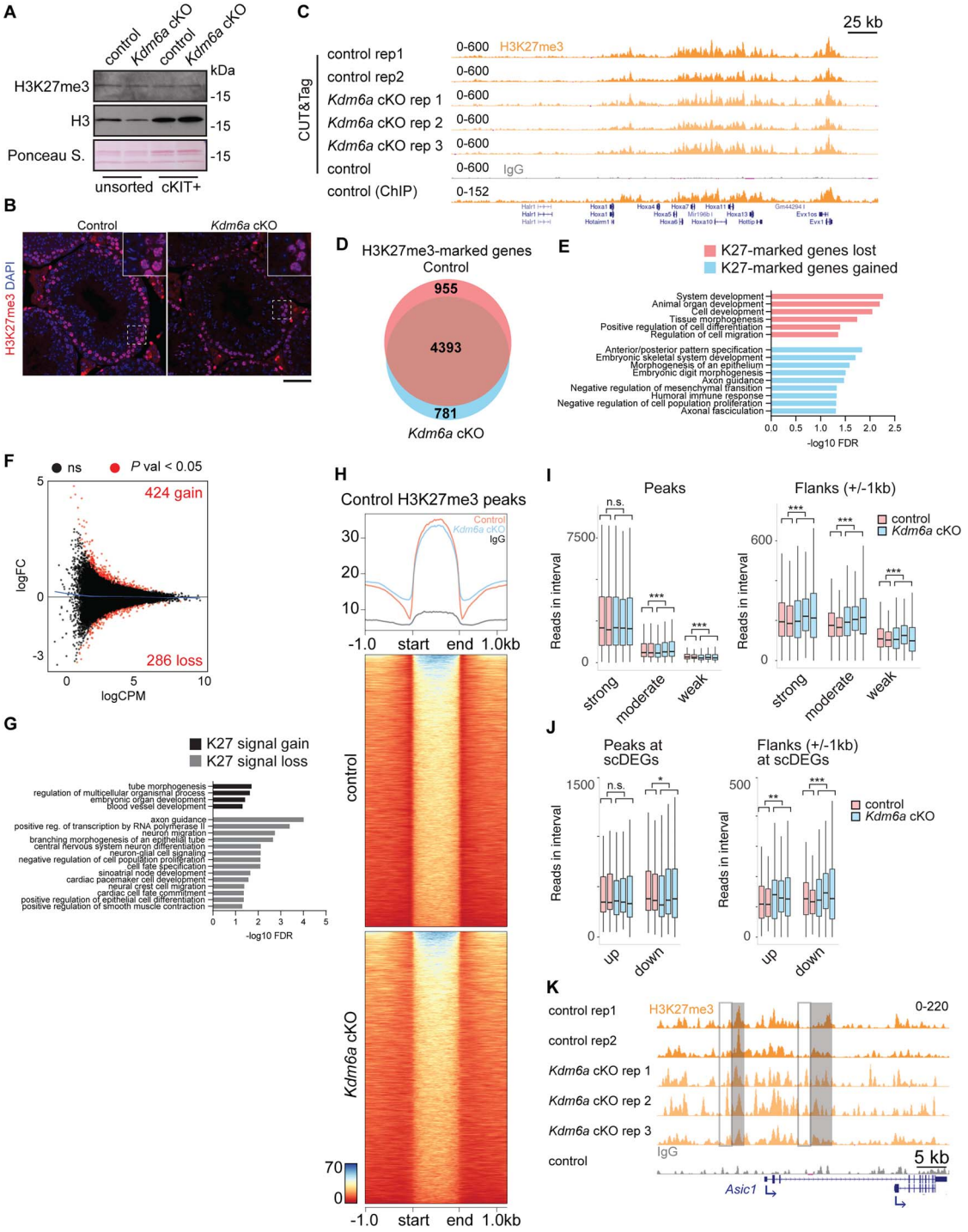

Figure 4. KDM6A regulates H3K27me3 distribution in differentiated spermatogonia. (**A**) Western blot for H3K27me3 and histone H3 in unsorted and cKIT+ cells from control and Kdm6a cKO testes. (**B**) Immunofluorescence detection of H3K27me3 in sections from control and *Kdm6a* cKO testis co-stained with DAPI. Scale bar = 50 μm. (**C**) Genome browser tracks at the Hox cluster showing representative signal for H3K27me3 in cKIT+ cells from control and *Kdm6a* cKO testes using CUT&Tag or ChIP-seq. IgG control sample demonstrates antibody specificity for H3K27me3 using CUT&Tag. (**D**) Overlap between genes marked by H3K27me3 in control and *Kdm6a* cKO cKIT+ cells. (**E**) Gene Ontology analysis for genes that lose and gain H3K27me3 in *Kdm6a* cKO cKIT+ cells. (**F**) MA plot for H3K27me3 peaks showing the distribution of differentially enriched peaks in *Kdm6a* cKO cKIT+ cells. Line is a loess fit to the distribution. (**G**) Gene Ontology enrichments for genes with differential H3K27me3 in *Kdm6a* cKO cKIT+ cells. (**H**) Top, metagene plot for average H3K27me3 signal at control-defined peaks in cKIT+ cells. Bottom, heat map showing individual traces for the same data. (**I**) Left, box plots for average read counts at strong, moderate, and weak H3K27me3 peaks in control and *Kdm6a* cKO cKIT+ cells; right, box plots for average read counts at the flanking regions (±1 kb) of strong, moderate, and weak H3K27me3 peaks. Boxes and lines represent the 25th, 50th, and 75th percentiles. Whiskers extend from the 10th to 90th percentiles. (**J**) Similar to (I) but specifically for the subset of peaks overlapping genes that are misregulated in the *Kdm6a* cKO. For panels (I) and (J), ns = not significant; $^{*}P < 0.05$; $^{**}P < 0.01$; $^{***}P < 0.001$ by quasi-Poisson regression (see Methods). (**K**) Genome browser track showing an example of H3K27me3 signal spreading in the *Kdm6a* cKO. Gray filled boxes cover peak regions and white boxes with a gray outline show sites where signal extends beyond the peak in *Kdm6a* cKO.

modification across the genome, and similar to the effect we previously observed for H3K27me3 in epididymal sperm of *Kdm6a* cKO males [14]. To better quantify this effect, we performed *k*-means clustering with $k = 3$ to define H3K27me3 peaks with strong ($n = 1498$), moderate ($n = 7256$), and weak ($n = 11{,}234$) signal, and counted reads within these peaks as well as in 1 kb upstream and downstream flanking regions, after down-sampling each library to match coverage depth across samples. We applied a regression model (see methods) to detect systematic differences between *Kdm6a* cKO and control across different genomic loci while accounting for variability across biological replicates. We detected no change in average signal within strong H3K27me3 peaks and a small but statistically significant decrease in signal in moderate and weak H3K27me3 peaks between *Kdm6a* cKO and control samples (Figure 4I). In contrast, we detected an overall increase in signal in flanking regions, with a pronounced and statistically significant increase in regions flanking H3K27me3 peaks regardless of signal strength (Figure 4I). H3K27me3 peaks associated with scDEGs followed the same pattern. There was no difference in H3K27me3 signal within peaks overlapping upregulated scDEGs, and a statistically significant but small decrease in signal within peaks overlapping downregulated scDEGs (Figure 4J and K). There was a pronounced and significant increase in H3K27me3 signal in regions flanking peaks at both upregulated and downregulated scDEGs (Figure 4J and K). Together, our results indicate that KDM6A is involved in demarcating the boundaries of H3K27me3 domains in differentiating spermatogonia, including at genes dependent on KDM6A for normal transcriptional regulation.

One possible effect of failure to set appropriate boundaries for H3K27me3 domains might be a switch from open, transcriptionally accessible chromatin to a closed, repressive state. To determine if defects in limiting H3K27me3 domains correspond to changes in chromatin accessibility, we next performed ATAC-seq in control ($n = 2$) and *Kdm6a* cKO ($n = 3$) cKIT+ spermatogenic cells isolated by flow cytometry. As expected, ATAC-seq peaks were predominantly located at promoters (Figure S6E and F). The set of genes associated with ATAC-seq peaks at promoters ($n = 7862$ promoters) was similar between control and *Kdm6a* cKO (Figure S6G and Data set S3). The small subset of promoters that gained ($n = 615$) and lost ($n = 206$) ATAC-seq peaks in *Kdm6a* cKO cells relative to control exhibited weak ATAC-seq signal and were poorly correlated with either scDEGs or sites of differential H3K27me3 signal (Data set S3). Quantitation of differences in ATAC-seq signal in the set of promoter-associated ATAC-seq peaks using the same pipeline used for H3K27me3 CUT&Tag data described above [69] identified only 24 regions that gained accessibility and 12 regions that lost accessibility at a threshold of $P < 0.01$ (Figure S6H). Therefore, the changes in H3K27me3 distribution induced in the absence of KDM6A do not appear to impact chromatin accessibility to regulate target genes.

A subset of genes is persistently deregulated in the germ lines of *Kdm6a* cKO males and their wild-type offspring

Somatic tissues of genetically wild-type mice derived from a paternal germ line lacking KDM6A ("*Kdm6a* F1s" see Figures 5A and S7A) exhibit transcriptomic and DNA methylation alterations [14]. These changes are greater in magnitude in the soma of wild-type mice that were derived from two successive generations in which the paternal germ line lacks KDM6A (*Kdm6a* F2s, Figures 5A and S7A), implying that KDM6A activity in the male germ line confers gene regulatory information that is additively perturbed over successive generations when germ line KDM6A activity is not restored. We therefore asked if gene expression differences could be detected in the male germ lines of *Kdm6a* F1 and *Kdm6a* F2 mice compared to control, reflecting aberrant retention of regulatory information.

We performed bulk RNA sequencing in whole testes of *Kdm6a* F1s ($n = 3$) and F2s ($n = 3$) as well as control F1s ($n = 3$, see Figures 5A and S7A) Principal component analysis of these data revealed differences in the transcriptomic profile between control, *Kdm6a* F1, and *Kdm6a* F2 testes (Figure 5B). Formal differential expression analysis of these data sets identified 85 DEGs for *Kdm6a* F1 compared to control F1 testes (P adj. ≤ 0.05, Data set S4 and Figure 5C), and 263 DEGs in *Kdm6a* F2 compared to control F1 testes (P adj. ≤ 0.05, Data set S4 and Figure 5C), while confirming that expression of *Kdm6a* itself is unaltered (Figure S7B). Our identification of more differentially expressed genes with higher statistical significance in the *Kdm6a* F2 compared to the *Kdm6a* F1 condition is consistent with a model where absence of KDM6A in the male germ line for two successive generations amplifies changes in gene regulatory state. In contrast to the scDEGs identified in the *Kdm6a* cKO germ line, we did not detect any bias in the direction of change in either *Kdm6a* F1 or F2 testis. Thirty-two DEGs detected in *Kdm6a* F1 or F2 testis were also identified as scDEGs in the *Kdm6a* cKO in our scRNA-seq data set (4% of all scDEGs, Data set S5), suggesting that a small subset of genes whose regulation is initially disrupted by loss of KDM6A in the parental germ line may be persistently deregulated across generations. However, only 10 genes were identified as DEGs in both *Kdm6a* F1 and F2 testes, likely because most changes in expression were small in magnitude and do not individually meet the significance threshold (Figure S7C). We therefore applied GSEA to test for global trends in expression across the entire set of scDEGs. This analysis revealed a significant (nominal $P < 0.0001$) enrichment for the set of downregulated, but not upregulated, scDEGs from *Kdm6a* cKO testis among the genes with altered expression in *Kdm6a* F1 or *Kdm6a* F2 whole testis (Figure 5D). This enrichment was greatest when using downregulated scDEGs from the "early pachytene" cluster as the testing gene set, corresponding to the timing of KDM6A expression and implying that many persistently deregulated genes may be direct targets of KDM6A in the male germ line (Figure S7D and E). The genes that contributed most to this effect ("leading edge genes") were enriched for meiotic processes and chromosome organization (Figure 5E). Notable examples of DEGs with persistent deregulation in testis across generations included genes that encode HUSH-associated proteins (*Tasor* and *Setdb1*) and histone demethylases (*Kdm5b* and *Kdm3a*) (Figure 5F).

Loss of histone demethylase-mediated regulation of repetitive elements in the parental germ line has been shown to adversely affect development of progeny in *Arabidopsis* [70]. Therefore, we also assessed repetitive element expression in our bulk RNA-seq data from testis of *Kdm6a* cKO, *Kdm6a* F1, and *Kdm6a* F2 males using an established pipeline [55]. We detected no differentially expressed repetitive elements in

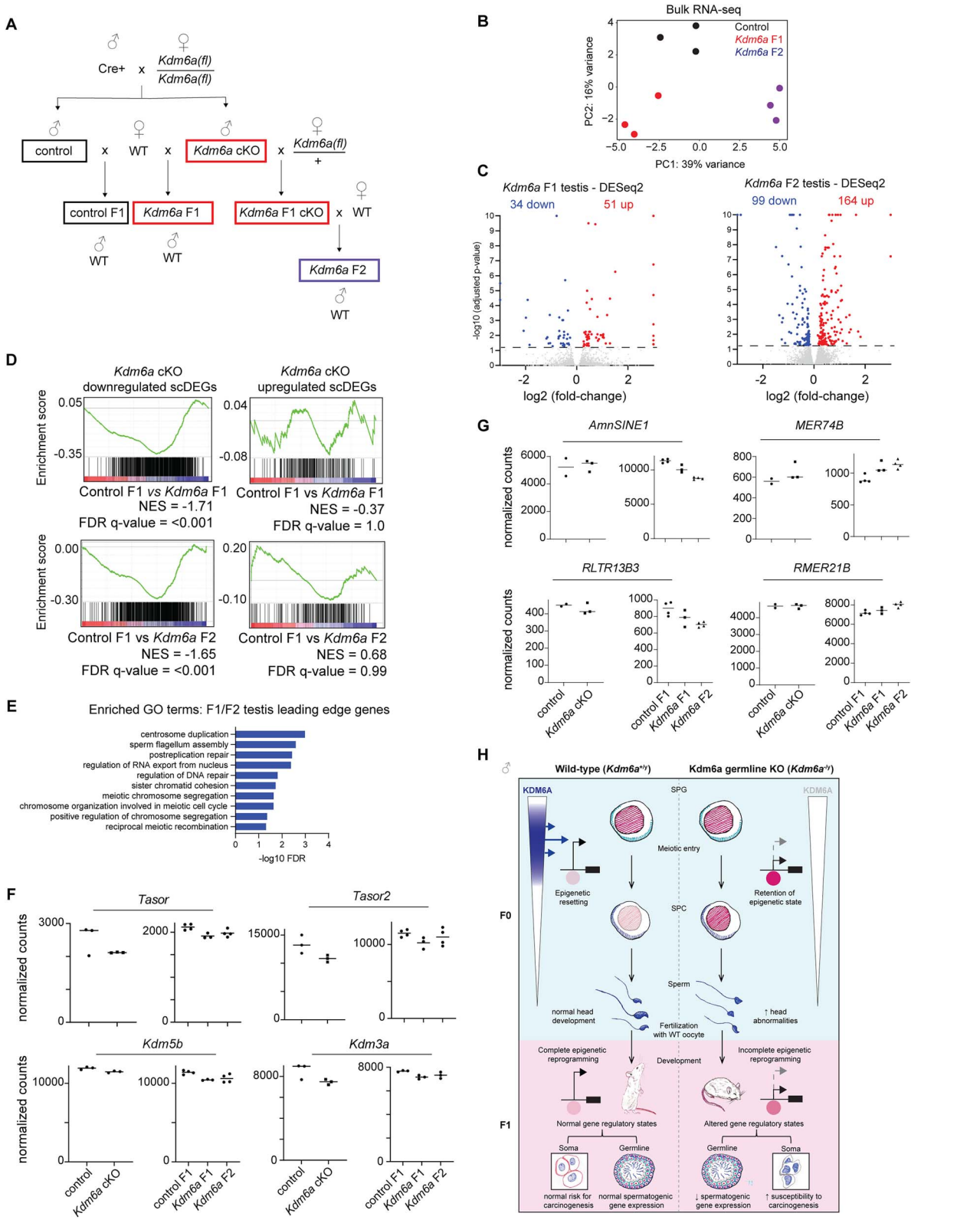

Figure 5. A subset of differentially expressed genes in the *Kdm6a* cKO germ line is persistently deregulated in testes of genetically wild-type offspring. (**A**) Simplified diagram showing breeding scheme for the generation of *Kdm6a* cKO mice and wild-type progeny (*Kdm6a* F1 and *Kdm6a* F2). (**B**) Principal component analysis for bulk RNA-seq data sets of control, *Kdm6a* F1, and *Kdm6a* F2 testis. (**C**) Volcano plot showing the gene expression changes in *Kdm6a* F1 testis (left) and *Kdm6a* F2 testis (right) relative to control F1 testes. (**D**) Gene set enrichment analysis (GSEA) plots showing enrichment for the set of scDEGs from *Kdm6a* cKO adult testes among genes with altered expression in the *Kdm6a* F1 (top) and *Kdm6a* F2 testis (bottom). The non-significant enrichment for upregulated scDEGs is shown by the GSEA plots to the right. NES, normalized enrichment score. (**E**) Gene Ontology terms enriched among "leading edge genes" from GSEA. (**F**) Normalized counts plotted for representative DEGs that are persistently deregulated across the germ lines of *Kdm6a* cKO, *Kdm6a* F1, and *Kdm6a* F2 mice. (**G**) Normalized counts plotted for four repetitive elements that are differentially expressed in the *Kdm6a* F1/F2 germ line. (**H**) Model for intergenerational inheritance of gene regulatory states following deletion of *Kdm6a* in the male germ line.

Kdm6a cKO testis, but identified four distinct repetitive elements (*AmnSINE1*, *MER74B*, *RLTR13B3*, *RMER21B*) that were differentially expressed in both *Kdm6a* F1 and *Kdm6a* F2 testis relative to control, with the extent of misregulation consistently greater in *Kdm6a* F2 compared to *Kdm6a* F1 data (Figure 5G). Together, we conclude that KDM6A activity in the male germ line contributes to regulation of expression of single-copy and repetitive loci in the germ lines of male offspring.

Discussion

Mice derived from a paternal germ line lacking *Kdm6a* have a reduced lifespan and more readily develop cancers [14]. Thus, KDM6A likely has activities in the male germ line that are important for gene regulation in the next generation. To identify these activities and begin to understand how they relate to offspring health, we evaluated the regulatory and phenotypic consequences of deleting *Kdm6a* in the postnatal male germ line. We found that KDM6A is expressed specifically and transiently in late spermatogonia and during early meiotic prophase, and that KDM6A loss perturbs gene regulatory programs that have lasting effects in late spermatogenesis and in germ cells of subsequent generations. These intergenerational effects are permitted in part because loss of KDM6A is compatible with normal sperm production and fertility (Figure 5H).

Although previous studies reported broad KDM6A expression across adult human and mouse seminiferous epithelium, including spermatocytes and round spermatids [71, 72], we found that *Kdm6a* expression at both the transcript and protein level was largely limited to late spermatogonia and the early stages of meiotic prophase. This discrepancy could be explained by cross-reactivity of anti-KDM6A antibodies in tissue sections. Indeed, we excluded several commercially sourced antibodies from our study due to nonspecific binding in cKO testis sections, and we were ultimately unable to identify an antibody that reliably reported KDM6A localization in mouse testis sections. Future immunolocalization of KDM6A in testis will be important to confirm the expression pattern we report here based on other evidence. Future experiments in which KDM6A is ectopically expressed in postmeiotic germ cells will also be of interest to better determine the significance of its restricted developmental expression.

Our *Kdm6a* cKO scRNA-seq data set revealed that the majority of changes in gene expression occurred in the same cell population that normally expresses KDM6A. Hence, these genes may represent direct targets of KDM6A regulatory activity. It will be important to obtain genome-wide profiles of KDM6A in cKIT+ spermatogenic cells to support this model [68]. Interestingly, we found that many of the expression changes that were detected early in spermatogenesis were also detected during late spermatogenesis in the *Kdm6a* cKO male germ line, implying that regulatory consequences of KDM6A loss extend throughout spermatogenic development even without continued expression of KDM6A. This effect could be perpetuated via an altered epigenetic state that is stable across meiosis and postmeiotic development. Previous work from our laboratory demonstrated broadening of H3K27me3 peaks in *Kdm6a* cKO epididymal sperm similar to that observed in cKIT+ differentiating spermatogonia in this study, suggesting that broadening of H3K27me3 domains may persist across spermatogenesis. The alterations to H3K27me3 that we observed in *Kdm6a* cKO spermatogonia may therefore represent the first induction of a retained defect in H3K27me3 distribution. Future work will determine if residual H3K27me3 is inherited by the zygote and if these domains are also inappropriately broadened relative to control.

In addition to its regulation of H3K27me3, KDM6A also cooperates with protein complexes containing members of the MLL family of histone methyltransferases to regulate methylation of H3K4 [31, 32]. Our *Kdm6a* cKO scRNA-seq data set also identified many differentially expressed genes encoding other epigenetic modifiers, raising the possibility of indirect changes to the chromatin landscape downstream of the gene regulatory activity of KDM6A. It will be of interest to determine if H3K4 methylation or other histone modifications are altered in the *Kdm6a* cKO germ line and whether they are associated with altered gene expression. Meanwhile, a causal link with H3K27me3 would best be made by analysis of knock-in mice bearing a catalytically dead version of KDM6A.

Our phenotyping of the *Kdm6a* cKO male germ line suggests that KDM6A does not have a critical role in spermatogenic development, but instead supports expression of genes encoding epigenetic modifiers and therefore shapes the histone methylome and heritable epigenome of germ cells and gametes. These results support a model where KDM6A is a regulator of epigenetic information more important for establishing the regulatory environment in the next generation than for paternal fertility. On the other hand, other histone demethylases may compensate for loss of KDM6A in spermatogenesis, masking a more overt function in fertility. We considered this possibility with KDM6B and UTY since both have been shown to function redundantly with KDM6A during mouse embryonic development and cellular differentiation, respectively [73, 74]. *Uty* transcript abundance is very low in testes, only partly overlaps in developmental timing with *Kdm6a*, and is not upregulated in the *Kdm6a* cKO, leading us to conclude that *Uty* likely does not compensate for *Kdm6a*. KDM6B expression does overlap with KDM6A and the phenotype of *Kdm6b* germline cKO males is similar: *Kdm6b* cKO males are fertile with higher numbers of undifferentiated spermatogonia [71]. Therefore, *Kdm6b* may be partially redundant with *Kdm6a* during spermatogenesis. In addition, the absence of changes in global levels of H3K27me3 in our *Kdm6a* cKO testes mirrors similar reports in the *Kdm6b*-null male germ line and further supports possible redundancy between these paralogs during spermatogenesis. KDM7B may also have some functional redundancy with KDM6A given that their expression profiles are very similar across spermatogenesis. Like *Kdm6a, Kdm7b* is X-linked in mammals and can demethylate H3K27 in zebrafish [63]. Definitive assessment of redundancies between KDM6A, UTY, KDM6B, and KDM7B in the male germ line will require generation of mice singly and multiply knocked out for each of these factors and comparative phenotyping at the cellular and molecular levels. If no spermatogenic defect is observed in males lacking multiple members of this family in the germ line, then it would be of interest to determine if intergenerational cancer risk in offspring is amplified relative to progeny of single *Kdm6a* knockouts.

We identified a small set of genes that was differentially expressed in both the male germ line of *Kdm6a* cKO

and in testes of genetically wild-type offspring. A similar phenomenon was recently reported in the male germ line of mice derived from a paternal germ line lacking *Scml2*, an X-linked gene that encodes a member of the Polycomb group of proteins [75]. Our results are consistent with a model in which KDM6A directly targets a specific set of genes to prevent inappropriate establishment of heritable epigenetic states. In the absence of KDM6A, these genes may acquire altered epigenetic states that are resistant to reprogramming and unable to be reset by KDM6A in the offspring. Such states would be expected to accumulate over multiple generations of a male germ line lacking KDM6A, consistent with our observation of more pronounced gene misregulation in testes of *Kdm6a* F2 compared to F1 animals.

Altogether, our analysis of spermatogenesis in *Kdm6a* cKO mice excludes sperm dysfunction as a primary explanation for the previously observed intergenerational effect on lifespan and cancer. Instead, we provide evidence supporting an intergenerational role for KDM6A activity in regulation of gene expression in the germ line by showing that some expression changes induced by KDM6A loss in spermatogenic cells are retained in the germ cells of subsequent generations, bypassing the resetting of acquired epigenetic information that ordinarily occurs soon after fertilization and during primordial germ cell development [76]. Our findings here echo studies in *C. elegans* showing that the status of H3K27me3 at paternal alleles is inherited across generations to regulate gene expression in the germ line [77]. A similar mechanism may be at play in our mammalian model. We speculate that loss of KDM6A in the male germ line permits accumulation of epimutations, some of which are resistant to erasure in the next generation and are difficult to reset even in the presence of a functional *Kdm6a* allele. Therefore, KDM6A may act during the dynamic chromatin reorganization that occurs at the start of meiosis to safeguard the male germ line from acquiring altered epigenetic states (Figure 5H). Future work will explore if altered H3K27me3 states are inherited by offspring, the mechanism by which they might resist reprogramming, and how such inherited epigenetic states could affect gene expression to confer cancer susceptibility.

Author contributions

BWW: conceptualization; methodology; validation; formal analysis; investigation; writing—original draft; visualization. SRR: formal analysis; visualization. RAH: formal analysis. ND: formal analysis. XH: investigation. DdeR: investigation. BJL: conceptualization; resources; writing—review and editing; visualization; supervision; project administration; funding acquisition.

Supplementary material

Supplementary material is available at *BIOLRE* online.

Acknowledgment

We thank P. Reddi for the gift of the ACRV1 antibody. We appreciate the technical assistance provided by Aushaq Malla, Allison Cho, Delaney Farris, Zachary Smith, and Jake Reske, and the help from the Yale Center for Genome Analysis for high-throughput sequencing. BWW is a Hope Funds for Cancer Research Fellow supported by the Hope Funds for Cancer Research (HFCR 22-03-04).

Conflict of interest: The authors have declared that no conflict of interest exists.

Data availability

All sequencing data sets can be found at the NCBI Gene Expression Omnibus data repository under accession number GSE215112.

References

1. Kuzmichev A, Nishioka K, Erdjument-Bromage H, Tempst P, Reinberg D. Histone methyltransferase activity associated with a human multiprotein complex containing the enhancer of Zeste protein. *Genes Dev* 2002; **16**:2893–2905.
2. Cao R, Wang L, Wang H, Xia L, Erdjument-Bromage H, Tempst P, Jones RS, Zhang Y. Role of histone H3 lysine 27 methylation in Polycomb-group silencing. *Science* 2002; **298**:1039–1043.
3. Boyer LA, Plath K, Zeitlinger J, Brambrink T, Medeiros LA, Lee TI, Levine SS, Wernig M, Tajonar A, Ray MK, Bell GW, Otte AP, *et al.* Polycomb complexes repress developmental regulators in murine embryonic stem cells. *Nature* 2006; **441**:349–353.
4. van Mierlo G, Dirks RAM, De Clerck L, Brinkman AB, Huth M, Kloet SL, *et al.* Integrative proteomic profiling reveals PRC2-dependent epigenetic crosstalk maintains ground-state pluripotency. *Cell Stem Cell* 2019; **24**:123–37.e8.
5. Mu W, Starmer J, Fedoriw AM, Yee D, Magnuson T. Repression of the soma-specific transcriptome by Polycomb-repressive complex 2 promotes male germ cell development. *Genes Dev* 2014; **28**:2056–2069.
6. Bernstein BE, Mikkelsen TS, Xie X, Kamal M, Huebert DJ, Cuff J, Fry B, Meissner A, Wernig M, Plath K, Jaenisch R, Wagschal A, *et al.* A bivalent chromatin structure marks key developmental genes in embryonic stem cells. *Cell* 2006; **125**:315–326.
7. Azuara V, Perry P, Sauer S, Spivakov M, Jørgensen HF, John RM, Gouti M, Casanova M, Warnes G, Merkenschlager M, Fisher AG. Chromatin signatures of pluripotent cell lines. *Nat Cell Biol* 2006; **8**:532–538.
8. Hammoud SS, Nix DA, Zhang H, Purwar J, Carrell DT, Cairns BR. Distinctive chromatin in human sperm packages genes for embryo development. *Nature* 2009; **460**:473–478.
9. Brykczynska U, Hisano M, Erkek S, Ramos L, Oakeley EJ, Roloff TC, Beisel C, Schübeler D, Stadler MB, Peters AHFM. Repressive and active histone methylation mark distinct promoters in human and mouse spermatozoa. *Nat Struct Mol Biol* 2010; **17**:679–687.
10. Sachs M, Onodera C, Blaschke K, Ebata KT, Song JS, Ramalho-Santos M. Bivalent chromatin marks developmental regulatory genes in the mouse embryonic germline in vivo. *Cell Rep* 2013; **3**:1777–1784.
11. Lesch BJ, Dokshin GA, Young RA, McCarrey JR, Page DC. A set of genes critical to development is epigenetically poised in mouse germ cells from fetal stages through completion of meiosis. *Proc Natl Acad Sci U S A* 2013; **110**:16061–16066.
12. Sakamoto M, Ito D, Inoue R, Wakayama S, Kikuchi Y, Yang L, Hayashi E, Emura R, Shiura H, Kohda T, Namekawa SH, Ishiuchi T, *et al.* Paternally inherited H3K27me3 affects chromatin accessibility in mouse embryos produced by round spermatid injection. *Development* 2022; **149**:18.
13. Kaneshiro KR, Rechtsteiner A, Strome S. Sperm-inherited H3K27me3 impacts offspring transcription and development in *C. elegans*. *Nat Commun* 2019; **10**:1271.
14. Lesch BJ, Tothova Z, Morgan EA, Liao Z, Bronson RT, Ebert BL, Page DC. Intergenerational epigenetic inheritance of cancer susceptibility in mammals. *Elife* 2019; **8**:e39380.
15. Siklenka K, Erkek S, Godmann M, Lambrot R, McGraw S, Lafleur C, Cohen T, Xia J, Suderman M, Hallett M, Trasler J, Peters AHFM, *et al.* Disruption of histone methylation in developing sperm impairs offspring health transgenerationally. *Science* 2015; **350**:aab2006.

16. Hong S, Cho YW, Yu LR, Yu H, Veenstra TD, Ge K. Identification of JmjC domain-containing UTX and JMJD3 as histone H3 lysine 27 demethylases. *Proc Natl Acad Sci U S A* 2007; **104**: 18439–18444.
17. Agger K, Cloos PA, Christensen J, Pasini D, Rose S, Rappsilber J, Issaeva I, Canaani E, Salcini AE, Helin K. UTX and JMJD3 are histone H3K27 demethylases involved in HOX gene regulation and development. *Nature* 2007; **449**:731–734.
18. Lan F, Bayliss PE, Rinn JL, Whetstine JR, Wang JK, Chen S, Iwase S, Alpatov R, Issaeva I, Canaani E, Roberts TM, Chang HY, *et al.* A histone H3 lysine 27 demethylase regulates animal posterior development. *Nature* 2007; **449**:689–694.
19. Sera Y, Nakata Y, Ueda T, Yamasaki N, Koide S, Kobayashi H, Ikeda KI, Kobatake K, Iwasaki M, Oda H, Wolff L, Kanai A, *et al.* UTX maintains the functional integrity of the murine hematopoietic system by globally regulating aging-associated genes. *Blood* 2021; **137**:908–922.
20. Jiang W, Wang J, Zhang Y. Histone H3K27me3 demethylases KDM6A and KDM6B modulate definitive endoderm differentiation from human ESCs by regulating WNT signaling pathway. *Cell Res* 2013; **23**:122–130.
21. Wang C, Lee JE, Cho YW, Xiao Y, Jin Q, Liu C, Ge K. UTX regulates mesoderm differentiation of embryonic stem cells independent of H3K27 demethylase activity. *Proc Natl Acad Sci U S A* 2012; **109**:15324–15329.
22. Lee S, Lee JW, Lee SK. UTX, a histone H3-lysine 27 demethylase, acts as a critical switch to activate the cardiac developmental program. *Dev Cell* 2012; **22**:25–37.
23. Mansour AA, Gafni O, Weinberger L, Zviran A, Ayyash M, Rais Y, Krupalnik V, Zerbib M, Amann-Zalcenstein D, Maza I, Geula S, Viukov S, *et al.* The H3K27 demethylase Utx regulates somatic and germ cell epigenetic reprogramming. *Nature* 2012; **488**: 409–413.
24. Dhar SS, Lee SH, Chen K, Zhu G, Oh W, Allton K, Gafni O, Kim YZ, Tomoiga AS, Barton MC, Hanna JH, Wang Z, *et al.* An essential role for UTX in resolution and activation of bivalent promoters. *Nucleic Acids Res* 2016; **44**:3659–3674.
25. Morales Torres C, Laugesen A, Helin K. Utx is required for proper induction of ectoderm and mesoderm during differentiation of embryonic stem cells. *PloS One* 2013; **8**:e60020.
26. Jiang Q, Huang X, Hu X, Shan Z, Wu Y, Wu G, Lei L. Histone demethylase KDM6A promotes somatic cell reprogramming by epigenetically regulating the PTEN and IL-6 signal pathways. *Stem Cells* 2020; **38**:960–972.
27. Yoo KH, Oh S, Kang K, Wang C, Robinson GW, Ge K, Hennighausen L. Histone demethylase KDM6A controls the mammary luminal lineage through enzyme-independent mechanisms. *Mol Cell Biol* 2016; **36**:2108–2120.
28. Welstead GG, Creyghton MP, Bilodeau S, Cheng AW, Markoulaki S, Young RA, Jaenisch R. X-linked H3K27me3 demethylase Utx is required for embryonic development in a sex-specific manner. *Proc Natl Acad Sci U S A* 2012; **109**:13004–13009.
29. Wang L, Shilatifard A. UTX mutations in human cancer. *Cancer Cell* 2019; **35**:168–176.
30. van Haaften G, Dalgliesh GL, Davies H, Chen L, Bignell G, Greenman C, Edkins S, Hardy C, O'Meara S, Teague J, Butler A, Hinton J, *et al.* Somatic mutations of the histone H3K27 demethylase gene UTX in human cancer. *Nat Genet* 2009; **41**: 521–523.
31. Wang SP, Tang Z, Chen CW, Shimada M, Koche RP, Wang LH, Nakadai T, Chramiec A, Krivtsov AV, Armstrong SA, Roeder RG. A UTX-MLL4-p300 transcriptional regulatory network coordinately shapes active enhancer landscapes for eliciting transcription. *Mol Cell* 2017; **67**:308–21.e6.
32. Gozdecka M, Meduri E, Mazan M, Tzelepis K, Dudek M, Knights AJ, Pardo M, Yu L, Choudhary JS, Metzakopian E, Iyer V, Yun H, *et al.* UTX-mediated enhancer and chromatin remodeling suppresses myeloid leukemogenesis through noncatalytic inverse regulation of ETS and GATA programs. *Nat Genet* 2018; **50**: 883–894.
33. Zehir A, Benayed R, Shah RH, Syed A, Middha S, Kim HR, Srinivasan P, Gao J, Chakravarty D, Devlin SM, Hellmann MD, Barron DA, *et al.* Mutational landscape of metastatic cancer revealed from prospective clinical sequencing of 10,000 patients. *Nat Med* 2017; **23**:703–713.
34. Gallardo T, Shirley L, John GB, Castrillon DH. Generation of a germ cell-specific mouse transgenic Cre line, Vasa-Cre. *Genesis* 2007; **45**:413–417.
35. Hu Y-C, de Rooij DG, Page DC. Tumor suppressor gene *Rb* is required for self-renewal of spermatogonial stem cells in mice. *Proc Natl Acad Sci U S A* 2013; **110**:12685–12690.
36. Gagnon KT, Li L, Janowski BA, Corey DR. Analysis of nuclear RNA interference in human cells by subcellular fractionation and Argonaute loading. *Nat Protoc* 2014; **9**:2045–2060.
37. Vasiliauskaitė L, Berrens RV, Ivanova I, Carrieri C, Reik W, Enright AJ, O'Carroll D. Defective germline reprogramming rewires the spermatogonial transcriptome. *Nat Struct Mol Biol* 2018; **25**: 394–404.
38. Bellvé AR. Purification, culture, and fractionation of spermatogenic cells. *Methods Enzymol* 1993; **225**:84–113.
39. Cunningham F, Allen JE, Allen J, Alvarez-Jarreta J, Amode MR, Armean IM, Austine-Orimoloye O, Azov AG, Barnes I, Bennett R, Berry A, Bhai J, *et al.* Ensembl 2022. *Nucleic Acids Res* 2022; **50**:D988–D995.
40. Bray NL, Pimentel H, Melsted P, Pachter L. Near-optimal probabilistic RNA-seq quantification. *Nat Biotechnol* 2016; **34**: 525–527.
41. Love MI, Huber W, Anders S. Moderated estimation of fold change and dispersion for RNA-seq data with DESeq2. *Genome Biol* 2014; **15**:550.
42. Hao Y, Hao S, Andersen-Nissen E, Mauck WM 3rd, Zheng S, Butler A, Lee MJ, Wilk AJ, Darby C, Zager M, Hoffman P, Stoeckius M, *et al.* Integrated analysis of multimodal single-cell data. *Cell* 2021; **184**:3573–87.e29.
43. Hannon G. FASTX-Toolkit Available from: http://hannonlab.cshl.edu/fastx_toolkit/index.html.
44. Martin M. Cutadapt removes adapter sequences from high-throughput sequencing reads. *FASTX-Toolkit* 2011; **17**:3.
45. Shen W, Le S, Li Y, Hu F. SeqKit: a cross-platform and ultrafast toolkit for FASTA/Q file manipulation. *PloS One* 2016; **11**:e0163962.
46. Langmead B, Salzberg SL. Fast gapped-read alignment with bowtie 2. *Nat Methods* 2012; **9**:357–359.
47. Li H, Handsaker B, Wysoker A, Fennell T, Ruan J, Homer N, Marth G, Abecasis G, Durbin R, 1000 Genome Project Data Processing Subgroup. The sequence alignment/map format and SAMtools. *Bioinformatics* 2009; **25**:2078–2079.
48. Ramírez F, Ryan DP, Grüning B, Bhardwaj V, Kilpert F, Richter AS, Heyne S, Dündar F, Manke T. deepTools2: a next generation web server for deep-sequencing data analysis. *Nucleic Acids Res* 2016; **44**:W160–W165.
49. Meers MP, Tenenbaum D, Henikoff S. Peak calling by sparse enrichment analysis for CUT&RUN chromatin profiling. *Epigenetics Chromatin* 2019; **12**:42.
50. Reske JJ, Wilson MR, Chandler RL. ATAC-seq normalization method can significantly affect differential accessibility analysis and interpretation. *Epigenetics Chromatin* 2020; **13**:22.
51. Dai Z, Sheridan JM, Gearing LJ, Moore DL, Su S, Wormald S, Wilcox S, O'Connor L, Dickins RA, Blewitt ME, Ritchie ME. edgeR: a versatile tool for the analysis of shRNA-seq and CRISPR-Cas9 genetic screens. *F1000Res* 2014; **3**:95.
52. Mi H, Huang X, Muruganujan A, Tang H, Mills C, Kang D, Thomas PD. PANTHER version 11: expanded annotation data from Gene Ontology and Reactome pathways, and data analysis tool enhancements. *Nucleic Acids Res* 2017; **45**:D183–D189.
53. Mootha VK, Lindgren CM, Eriksson K-F, Subramanian A, Sihag S, Lehar J, Puigserver P, Carlsson E, Ridderstråle M, Laurila E, Houstis N, Daly MJ, *et al.* PGC-1α-responsive genes involved in oxidative phosphorylation are coordinately downregulated in human diabetes. *Nat Genet* 2003; **34**:267–273.

54. Subramanian A, Tamayo P, Mootha VK, Mukherjee S, Ebert BL, Gillette MA, Paulovich A, Pomeroy SL, Golub TR, Lander ES, Mesirov JP. Gene set enrichment analysis: a knowledge-based approach for interpreting genome-wide expression profiles. *Proc Natl Acad Sci* 2005; **102**:15545–15550.
55. Criscione SW, Zhang Y, Thompson W, Sedivy JM, Neretti N. Transcriptional landscape of repetitive elements in normal and cancer human cells. *BMC Genomics* 2014; **15**:583.
56. Ver Hoef JM, Boveng PL. Quasi-Poisson vs. negative binomial regression: how should we model overdispersed count data? *Ecology* 2007; **88**:2766–2772.
57. Greenfield A, Carrel L, Pennisi D, Philippe C, Quaderi N, Siggers P, Steiner K, Tam PP, Monaco AP, Willard HF, Koopman P. The UTX gene escapes X inactivation in mice and humans. *Hum Mol Genet* 1998; **7**:737–742.
58. Hofmann MC, Narisawa S, Hess RA, Millán JL. Immortalization of germ cells and somatic testicular cells using the SV40 large T antigen. *Exp Cell Res* 1992; **201**:417–435.
59. Jung M, Wells D, Rusch J, Ahmad S, Marchini J, Myers SR, Conrad DF. Unified single-cell analysis of testis gene regulation and pathology in five mouse strains. *Elife* 2019; **8**:e43966.
60. Guo J, Grow EJ, Mlcochova H, Maher GJ, Lindskog C, Nie X, Guo Y, Takei Y, Yun J, Cai L, Kim R, Carrell DT, *et al.* The adult human testis transcriptional cell atlas. *Cell Res* 2018; **28**:1141–1157.
61. Yoshinaga K, Nishikawa S, Ogawa M, Hayashi S, Kunisada T, Fujimoto T, Nishikawa SI. Role of c-kit in mouse spermatogenesis: identification of spermatogonia as a specific site of c-kit expression and function. *Development* 1991; **113**:689–699.
62. Russell LD (ed.). *Histological and Histopathological Evaluation of the Testis*. Clearwater, FL: Cache River Press, 1990.
63. Tsukada Y, Ishitani T, Nakayama KI. KDM7 is a dual demethylase for histone H3 Lys 9 and Lys 27 and functions in brain development. *Genes Dev* 2010; **24**:432–437.
64. Amann RP, Waberski D. Computer-assisted sperm analysis (CASA): capabilities and potential developments. *Theriogenology* 2014; **81**:5–17.e1-3.
65. Douse CH, Tchasovnikarova IA, Timms RT, Protasio AV, Seczynska M, Prigozhin DM, Albecka A, Wagstaff J, Williamson JC, Freund SMV, Lehner PJ, Modis Y. TASOR is a pseudo-PARP that directs HUSH complex assembly and epigenetic transposon control. *Nat Commun* 2020; **11**:4940.
66. Tchasovnikarova IA, Timms RT, Douse CH, Roberts RC, Dougan G, Kingston RE, *et al.* Hyperactivation of HUSH complex function by Charcot–Marie–Tooth disease mutation in MORC2. *Nat Genet* 2017; **49**:1035–1044.
67. Lee MG, Villa R, Trojer P, Norman J, Yan KP, Reinberg D, di Croce L, Shiekhattar R. Demethylation of H3K27 regulates polycomb recruitment and H2A ubiquitination. *Science* 2007; **318**:447–450.
68. Kaya-Okur HS, Wu SJ, Codomo CA, Pledger ES, Bryson TD, Henikoff JG, Ahmad K, Henikoff S. CUT&Tag for efficient epigenomic profiling of small samples and single cells. *Nat Commun* 2019; **10**:1930.
69. Stark R, Brown G. DiffBind: differential binding analysis of ChIP-Seq peak data. *R package version* 2011; **100**.
70. Antunez-Sanchez J, Naish M, Ramirez-Prado JS, Ohno S, Huang Y, Dawson A, Opassathian K, Manza-Mianza D, Ariel F, Raynaud C, Wibowo A, Daron J, *et al.* A new role for histone demethylases in the maintenance of plant genome integrity. *Elife* 2020; **9**:e58533.
71. Iwamori N, Iwamori T, Matzuk MM. H3K27 demethylase, JMJD3, regulates fragmentation of spermatogonial cysts. *PloS One* 2013; **8**:e72689.
72. Vogt PH, Zimmer J, Bender U, Strowitzki T. AZFa candidate gene UTY and its X homologue UTX are expressed in human germ cells. *Reprod Fertil* 2021; **2**:151–160.
73. Shpargel KB, Sengoku T, Yokoyama S, Magnuson T. UTX and UTY demonstrate histone demethylase-independent function in mouse embryonic development. *PLoS Genet* 2012; **8**: e1002964.
74. Manna S, Kim JK, Baugé C, Cam M, Zhao Y, Shetty J, Vacchio MS, Castro E, Tran B, Tessarollo L, Bosselut R. Histone H3 lysine 27 demethylases Jmjd3 and Utx are required for T-cell differentiation. *Nat Commun* 2015; **6**:8152.
75. Sakashita A, Ooga M, Otsuka K, Maezawa S, Takeuchi C, Wakayama S, Wakayama T, Namekawa SH. Polycomb protein SCML2 mediates paternal epigenetic inheritance through sperm chromatin. *Nucleic Acids Res* 2023; **51**:6668–6683.
76. Cantone I, Fisher AG. Epigenetic programming and reprogramming during development. *Nat Struct Mol Biol* 2013; **20**:282–289.
77. Kaneshiro KR, Egelhofer TA, Rechtsteiner A, Cockrum C, Strome S. Sperm-inherited H3K27me3 epialleles are transmitted transgenerationally in cis. *Proc Natl Acad Sci U S A* 2022; **119**:e2209471119.